P5.6 **A SCALE-DISCRIMINATING VORTICITY BUDGET FOR A MESOSCALE CONVECTIVE VORTEX**

Jason C. Knievel* and Richard H. Johnson
Colorado State University, Fort Collins, Colorado

1. INTRODUCTION

Mesoscale convective systems (MCSs) sometimes generate mesoscale convective vortices (MCVs) in the lower and middle troposphere. If friction is ignored, vertical vorticity within an MCV must originate from some combination of a) horizontal advection of absolute vorticity, b) vertical advection of relative vorticity, c) convergence of absolute vorticity, d) tilting of horizontal vorticity by horizontally varying vertical wind, and e) horizontal baroclinity.

These sources and sinks of vorticity exist within an MCS's mesoscale circulations as well as within the environment's synoptic circulations yet, to date, no empirical vorticity budget for an MCV has discriminated between the two scales. An MCS and MCV that formed on 1 August 1996 afforded the opportunity for a scale-discriminating vorticity budget when they traversed the densest part of the National Oceanic and Atmospheric Administration Wind Profiler Network (NPN) in Kansas and Oklahoma.

Another paper of ours in this volume provides an overview of the MCS's lifecycle. Please refer to that paper for depictions of radar reflectivity and mesoscale wind fields.

2. DATA AND METHODS

Kinematical soundings are from the NPN, radiosondes launched semi-daily by the National Weather Service, and radiosondes launched every three hours from four sites in Oklahoma as part of 1996's Enhanced Seasonal Observing Period (ESOP-96) of the Global Energy and Water Cycle Experiment's (GEWEX's) Continental-Scale International Project (GCIP).

Over the period of detailed analysis, 0900–1800 UTC on 1 August, 12% of soundings were missing at the NPN sites closest to the MCS; 13% were missing at the seven most densely spaced sites in Oklahoma and Kansas.

To produce gridded fields of *total wind*, $\boldsymbol{u}(u, v, w)$, we used a two-pass Barnes analysis (Barnes 1973; Koch et al. 1983) on data from the NPN. Grid points were 75 km apart, and the response function was chosen to capture 90% of the signal of phenomena with wavelengths of 300 km (*total* curve in fig. 1). We then employed a second Barnes analysis that, together with the first, acted as a bandpass filter (Maddox 1980). The *synoptic background wind*, $\widetilde{\boldsymbol{u}}(\widetilde{u}, \widetilde{v}, \widetilde{w})$, was approximated with data filtered to include 90% and 0.09% of the signals of phenomena with wavelengths of 1600 km and 300 km, respectively (*synoptic* curve in fig. 1). The *mesoscale perturbation in wind*, $\widehat{\boldsymbol{u}}(\widehat{u}, \widehat{v}, \widehat{w})$, was approximated by subtracting the synoptic background wind from the total wind (*mesoscale* curve in fig. 1).

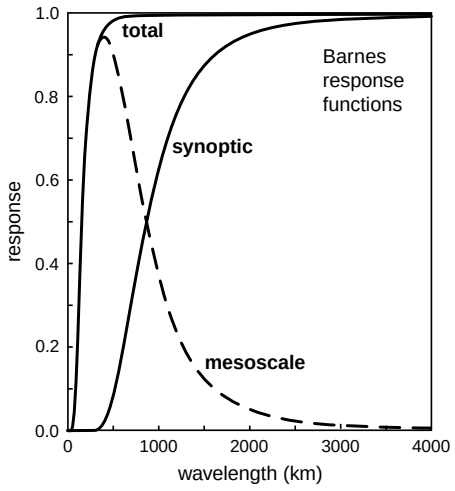

Figure 1: Response functions for the Barnes analyses.

We calculated divergence and vorticity from centered finite differences of gridded wind. Vertical velocity is from the kinematic method with a linear correction to density-weighted divergence (O'Brien 1970), for which we set $w = 0$ at 750 m above the tropopause and $w = 0$ at 500 m above ground level (AGL).

Baroclinity is weak near MCVs and can be ignored without much inaccuracy (Skamarock et al. 1994). For the remaining sources and sinks of vorticity we calculated a budget for the synoptic background wind and the mesoscale perturbation in wind. Calculations were for 3-h periods over a $2^\circ \times 2^\circ$ area centered on the MCV in the middle troposphere. Because of unresolved sources and sinks of vorticity, the budget has a residual, which

Addresses of the corresponding author: Jason C. Knievel, Department of Atmospheric Science, Colorado State University, Fort Collins, CO 80523-1371; knievel@atmos.colostate.edu

also includes observational errors. When written in terms of the resolved synoptic component, ($\widetilde{\ }$); the resolved mesoscale component, ($\widehat{\ }$); and the residual, Z, the vertical vorticity equation for inviscid flow is

$$\begin{aligned}\frac{\partial\zeta}{\partial t} = &-(\widetilde{\boldsymbol{v}}+\widehat{\boldsymbol{v}})\cdot\boldsymbol{\nabla}(\widetilde{\zeta}+f+\widehat{\zeta})\\ &-(\widetilde{w}+\widehat{w})\frac{\partial(\widetilde{\zeta}+\widehat{\zeta})}{\partial z}\\ &-(\widetilde{\zeta}+f+\widehat{\zeta})\boldsymbol{\nabla}\cdot(\widetilde{\boldsymbol{v}}+\widehat{\boldsymbol{v}})\\ &+(\widetilde{\xi}+\widehat{\xi})\frac{\partial(\widetilde{w}+\widehat{w})}{\partial x}+(\widetilde{\eta}+\widehat{\eta})\frac{\partial(\widetilde{w}+\widehat{w})}{\partial y}\\ &+\mathbf{J}_{\mathbf{xy}}(\widetilde{p}+\widehat{p},\widetilde{\alpha}+\widehat{\alpha})\\ &+Z,\end{aligned} \tag{1}$$

wherein $\boldsymbol{\zeta}(\xi,\eta,\zeta)$ is relative vorticity, $\boldsymbol{v}(u,v)$ is horizontal wind, w is vertical wind, f is the Coriolis parameter, and $\mathbf{J}_{\mathbf{xy}}\,(p,\alpha)$ is the two-dimensional Jacobian of pressure, p, and specific volume, α. (Hereafter, *vorticity* means *relative vertical vorticity*, and *divergence* and *convergence* mean *horizontal divergence* and *horizontal convergence* unless otherwise stated.)

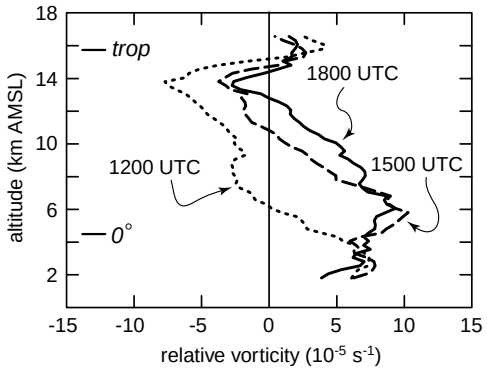

Figure 2: Relative vorticity (10^{-5} s^{-1}) in the total wind at 1200 (dotted), 1500 (dashed), and 1800 UTC (solid). Profiles are for a $2^\circ\times2^\circ$ area centered on the MCV in the middle troposphere, averaged over 3 h ending at the time labeled.

3. VORTICITY BUDGET

Over the nine hours we examined, the MCV deepened and strengthened as the MCS matured and decayed, until the MCV occupied almost the entire troposphere (fig. 2). Convergence, tilting, and unresolved effects within the total wind contributed the most to the MCV's growth.

Between 0900 and 1200 UTC there were only two positive sources of vorticity from 2 to 4 km above mean sea level (AMSL), which was the layer of maximum vorticity in the MCV: tilting (fig. 3a) and unresolved effects (fig. 4). Because the MCV had already formed by the start of the period of analysis, we could not determine the source of vorticity for the incipient vortex. Even so, figure 3a suggests that tilting may have played the largest role on resolvable scales, which would be consistent with work by Zhang (1992) and Davis and Weisman (1994).

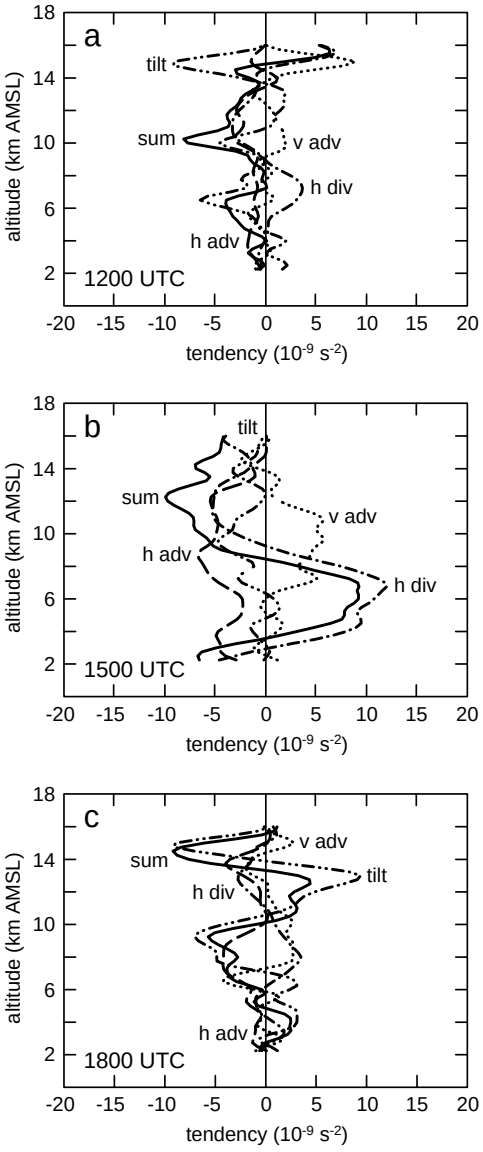

Figure 3: Resolved part of the vorticity budget for the total wind on 1 August 1996. Terms are: horizontal advection (dashed), vertical advection (dotted), horizontal divergence (dot-dashed), tilting (dot-dot-dashed), and the sum of terms (solid). Profiles are for a $2^\circ\times2^\circ$ area centered on the MCV in the middle troposphere, averaged over 3 h ending at a) 1200, b) 1500, and c) 1800 UTC.

The MCV of 1 August 1996 grew deeper and stronger between 1200 and 1500 UTC primarily from convergence of positive absolute vorticity in the middle troposphere (fig. 3b). Planetary and relative vorticities con-

tributed almost equally (not shown). If not for divergence of planetary vorticity in the upper troposphere, the tendency due to divergence there at 1500 UTC would have been positive as well, because upper-tropospheric relative vorticity was negative (fig. 2). Indeed, because divergence and relative vorticity were approximately anticorrelated about zero (not shown), any deep layers of negative tendency due to divergence must have been from divergent wind acting on planetary vorticity, because divergence of negative relative vorticity and convergence of positive relative vorticity cannot produce a negative tendency. Davis and Weisman (1994) alluded to this. At the same time that convergence of absolute vorticity generated vorticity in the lower and middle troposphere, the mesoscale updraft advected that vorticity upward (fig. 3b). However, positive vertical advection of vorticity was overwhelmed by all the other resolved sinks. In particular, horizontal advection decreased vorticity from the lower through the upper troposphere.

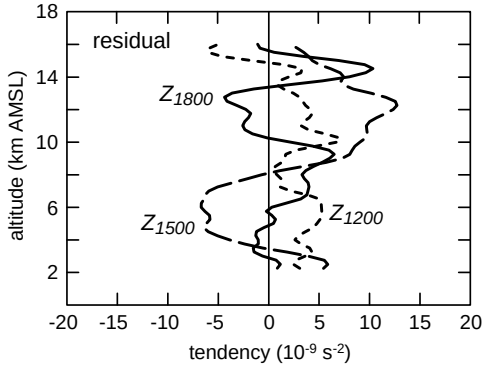

Figure 4: Vorticity tendency due to the residual in the total wind at 1200 UTC (short dashed), 1500 UTC (long dashed), and 1800 UTC (solid) on 1 August 1996. Profiles are for a $2^\circ \times 2^\circ$ area centered on the MCV in the middle troposphere, averaged over 3 h ending at the time labeled.

Convergence between 1200 and 1500 UTC was likely aided by the existent MCV's vorticity because of its effect on the Rossby radius of deformation,

$$\lambda_R = \frac{NH}{(\zeta + f)^{1/2} (2VR^{-1} + f)^{1/2}}, \qquad (2)$$

wherein N is the Brunt-Väisällä frequency, H is the scale height of the disturbance, ζ is the vertical component of relative vorticity, f is the Coriolis parameter, and V is the wind's rotational component, of which R is the radius of curvature (Frank 1983). How the atmosphere responds to heating by phase changes in water within a stratiform region depends partly on the horizontal size of the heated area compared with λ_R. When sources of diabatic heating are larger than λ_R, more energy is retained in balanced, vortical flow near an MCS than is transmitted to the far field by gravity waves and buoyancy rolls (Mapes 1993; Schubert et al. 1980), and the transition to balanced, vortical flow involves convergence. Background vorticity shrinks λ_R, and the incipient MCV of 1 August 1996 supplied that background vorticity. At 0800 UTC, close to the time when a vortical circulation was first visible in loops of reflectivity, λ_R was 276 km, which is close to the 280 km calculated by Chen and Frank (1993) and the 300 km calculated by Cotton et al. (1989) for MCS environments. By 1200 UTC, λ_R had shrunk to 136 km. It stayed close to that value through 1500 UTC, the interval of maximum strengthening of the MCV. We estimate the radius of maximum wind for the MCV was 1° of latitude (111 km). The size of the stratiform region is harder to estimate, but the major axis was perhaps 350 km long during the asymmetric stage of the MCS, giving a pseudo-radius of 175 km. This is slightly larger than λ_R, so a large fraction of the atmosphere's response to heating was retained near the MCS as convergent and vortical flow in the middle troposphere between 1200 and 1500 UTC.

Tilting was the main source of the vorticity in the upper troposphere that further deepened the MCV during the final three hours of the period of analysis (fig. 3c). Tilting and convergence were the main sources of vorticity in the lower troposphere. The MCV was partially maintained in the middle troposphere by unresolved effects represented by the residual (fig. 4) and by convergence of absolute vorticity. Three-dimensional advection was generally a sink of vorticity at 6 km AMSL, the altitude of maximum vorticity in the MCV (fig. 3c).

A few general properties of the vorticity budget deserve mention. In agreement with observations by Chong and Bousquet (1999) and others, tilting and vertical advection of vorticity were roughly anticorrelated about zero (fig. 3). Only when this anticorrelation broke down did tilting and vertical advection play large, net roles in the local tendency. The often similar anticorrelation between horizontal advection and divergence of vorticity was weaker, yet discernible. Unresolved effects represented by the residual were as large as those explicitly resolved in the budget (cf. figs. 3 and 4), which strongly suggests that regions of persistent convective-scale circulations altered atmospheric vorticity on the mesoscale.

When terms in (1) are separated into their synoptic and mesoscale components (see the following subsections), the budget exemplifies commonly observed—in some cases defining—traits of synoptic and mesoscale motions. Within the mesoscale component, the magnitudes of three-dimensional wind speeds, divergence, and vorticity were all large. Within the synoptic component, the magnitudes of vertical velocity and divergence were comparatively small.

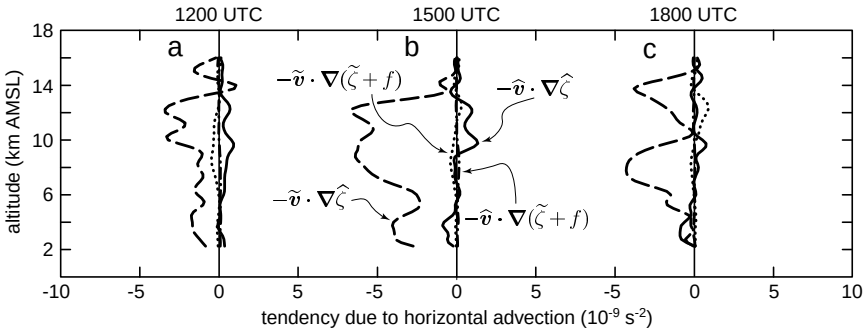

Figure 5: Vorticity tendency due to components of horizontal advection on 1 August 1996.

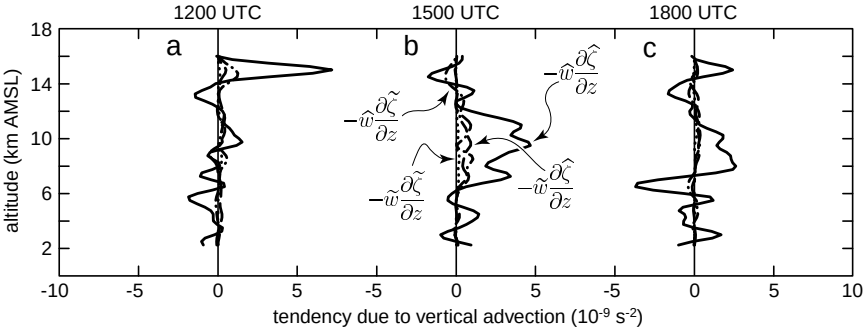

Figure 6: Vorticity tendency due to components of vertical advection on 1 August 1996.

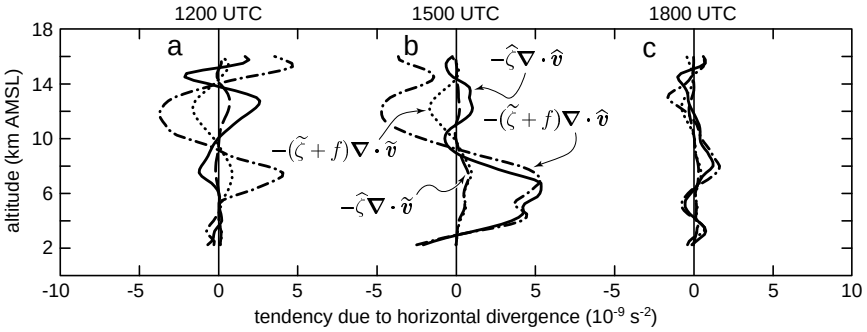

Figure 7: Vorticity tendency due to components of horizontal divergence on 1 August 1996.

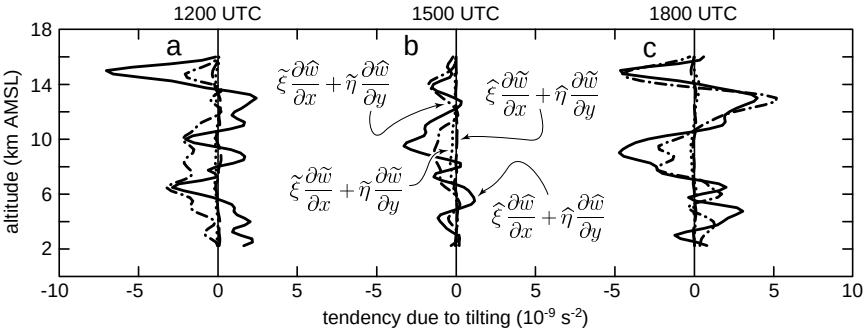

Figure 8: Vorticity tendency due to components of tilting on 1 August 1996. All profiles on this page are for a $2^\circ \times 2^\circ$ area centered on the MCV in the middle troposphere, averaged over 3 h ending at the time labeled.

3.1 *Tendency from horizontal advection*

Nearly all the vorticity tendency from horizontal advection was due to advection of mesoscale vorticity by the synoptic wind (fig. 5). The reason horizontal advection of mesoscale vorticity by the mesoscale wind was so small is that in the vortical flow of the MCV the gradient of mesoscale vorticity was nearly orthogonal to the mesoscale wind, so horizontal advection was very weak even though the two parts of the advection term were large. Gradients of synoptic vorticity were too small to permit much horizontal advection, even though synoptic vorticity was as large as mesoscale vorticity because we included planetary vorticity in the former.

3.2 *Tendency from vertical advection*

Nearly all the vorticity tendency from vertical advection was due to advection of mesoscale vorticity by the mesoscale wind (fig. 6). Not surprisingly, the only vertical motions strong enough to contribute much to vertical advection were in the mesoscale field. Synoptic vorticity, while large, did not lead to large vertical advection even by the mesoscale wind because vertical gradients of synoptic vorticity were small.

3.3 *Tendency from horizontal divergence*

No component in the vorticity tendency from horizontal divergence was negligibly small, although two components were dominant (fig. 7). From 1200 to 1500 UTC, when the MCV underwent the greatest deepening and strengthening, vorticity in the MCV was generated mostly, and nearly equally, by convergence of mesoscale vorticity and convergence of synoptic vorticity, both by the mesoscale wind. Tendency due to convergence of synoptic vorticity by the synoptic wind was at least a factor of one-half smaller than the dominant terms, and tendency due to convergence of mesoscale vorticity by the synoptic wind was smaller yet, especially in the upper troposphere.

3.4 *Tendency from tilting*

Finally, the only two components that contributed appreciably to the vorticity tendency from tilting were tilting of both synoptic and mesoscale vorticity by horizontally varying mesoscale updrafts (fig. 8). Synoptic updrafts were too weak, and their horizontal variations too small, to provide much torque on tubes of horizontal vorticity. Tilted horizontal vorticity consistently contained large synoptic as well as mesoscale components. This differs somewhat from the study by Davis and Weisman (1994), in which they found that tilting of environmental shear was dominant early in a simulated MCS, but was later exceeded by tilting of perturbation vorticity.

Acknowledgments. The National Science Foundation supported this research with grants ATM 9618684 and ATM 0071371, the National Aeronautics and Space Administration with grant NCC5-288 SUPP 0002.

REFERENCES

Barnes, S. L., 1973: Mesoscale objective analysis using weighted time-series observations. NOAA Tech. Memo. ERL NSSL-62, National Severe Storms Laboratory, Norman, OK, 60 pp. [NTIS COM-73-10781. Available from National Severe Storms Laboratory, Norman, OK 73069.]

Chen, S. S., and W. M. Frank, 1993: A numerical study of the genesis of extratropical convective mesovortices. Part I: Evolution and dynamics. *J. Atmos. Sci.*, **50**, 2401–2426.

Chong, M., and O. Bousquet, 1999: A mesovortex within a near-equatorial mesoscale convective system during TOGA COARE. *Mon. Wea. Rev.*, **127**, 1145–1156.

Cotton, W. R., M. S. Lin, R. L. McAnelly, and C. J. Tremback, 1989: A composite model of mesoscale convective complexes. *Mon. Wea. Rev.*, **117**, 765–783.

Davis, C. A., and M. L. Weisman, 1994: Balanced dynamics of mesoscale vortices produced in simulated convective systems. *J. Atmos. Sci.*, **51**, 2005–2030.

Frank, W. M., 1983: The cumulus parameterization problem. *Mon. Wea. Rev.*, **111**, 1859–1871.

Koch, S. E., M. DesJardins, and P. J. Kocin, 1983: An interactive Barnes objective map analysis scheme for use with satellite and conventional data. *J. Climate Appl. Meteor.*, **22**, 1487–1503.

Maddox, R. A., 1980: An objective technique for separating macroscale and mesoscale features in meteorological data. *Mon. Wea. Rev.*, **108**, 1108–1121.

Mapes, B. E., 1993: Gregarious tropical convection. *J. Atmos. Sci.*, **50**, 2026–2037.

O'Brien, J. J., 1970: Alternative solutions to the classical vertical velocity problem. *J. Appl. Meteor.*, **9**, 197–203.

Schubert, W. H., J. J. Hack, P. L. Silva Dias, and S. R. Fulton, 1980: Geostrophic adjustment in an axisymmetric vortex. *J. Atmos. Sci.*, **37**, 1464–1484.

Skamarock, W. C., M. L. Weisman, and J. B. Klemp, 1994: Three-dimensional evolution of simulated long-lived squall lines. *J. Atmos. Sci.*, **51**, 2563–2584.

Zhang, D.-L., 1992: The formation of a cooling-induced mesovortex in the trailing stratiform region of a midlatitude squall line. *Mon. Wea. Rev.*, **120**, 2763–2785.